SCIENTIFIC REPORTS

OPEN

SUBJECT AREAS:
ORGANIC-INORGANIC NANOSTRUCTURES
NANOSENSORS
BIOANALYTICAL CHEMISTRY
ELECTROCATALYSIS

Received
19 September 2014

Accepted
4 December 2014

Published
9 January 2015

Correspondence and requests for materials should be addressed to Y.L. (yingchunli_judy@163.com) or Y.D. (yding@sdu.edu.cn)

Molecularly imprinted polymer decorated nanoporous gold for highly selective and sensitive electrochemical sensors

Yingchun Li[1], Yuan Liu[1], Jie Liu[1], Jiang Liu[1], Hui Tang[1], Cong Cao[4], Dongsheng Zhao[4] & Yi Ding[2,3]

[1]School of Pharmacy, Shihezi University, Shihezi 832000, China, [2]Institute for New Energy Materials and Low-Carbon Technologies, and School of Materials Science and Engineering, Tianjin University of Technology, Tianjin 300384, China, [3]Center for Advanced Energy Materials & Technology Research (AEMT), and School of Chemistry and Chemical Engineering, Shandong University, Jinan 250100, China, [4]Nano Laboratory, Shandong Institute of Metrology, Jinan 250014, China.

Electrochemical nanosensors based on nanoporous gold leaf (NPGL) and molecularly imprinted polymer (MIP) are developed for pharmaceutical analysis by using metronidazole (MNZ) as a model analyte. NPGL, serving as the loading platform for MIP immobilization, possesses large accessible surface area with superb electric conductivity, while electrochemically synthesized MIP thin layer affords selectivity for specific recognition of MNZ molecules. For MNZ determination, the hybrid electrode shows two dynamic linear range of 5×10^{-11} to 1×10^{-9} mol L^{-1} and 1×10^{-9} to 1.4×10^{-6} mol L^{-1} with a remarkably low detection limit of 1.8×10^{-11} mol L^{-1} (S/N=3). In addition, the sensor exhibits high binding affinity and selectivity towards MNZ with excellent reproducibility and stability. Finally, the reliability of MIP-NPGL for MNZ detection is proved in real fish tissue samples, demonstrating the potential for the proposed electrochemical sensors in monitoring drug and biological samples.

Metronidazole (MNZ) is a nitroimidazole derivative and has been widely used for the treatment of protozoal diseases including Giardia infections, amebic liver abscess, bacterial vaginosis[1,2], etc. In general, MNZ is also employed for any potentially susceptible anaerobic infection by veterinary community or as a promoter to induce the growth of aquatic products[3–5]. However, MNZ has been banned by many countries and areas from use in food producing animals[6] due to its carcinogenic properties according to the WHO International Agency for Research on Cancer (IARC)[7]. In view of the above, accurate and reliable analytical methods for the determination of MNZ in various samples are crucial for food security, human health and investigations on the biological toxicity of MNZ.

Different methods have been developed for this purpose, most of which are on the basis of chromatography[8], spectrophotometry[9–11], and electrochemistry[4,5,12–22]. Among them, the latter approach has some admirable characteristics like easy preparation, low cost, simple sample manipulation, high sensitivity and rapid response[23]. Hence, modification of electrochemical electrode with highly selective and sensitive agents has attracted much attention in monitoring MNZ[4,5,12–22].

Molecularly imprinted polymers (MIPs), commonly viewed as synthetic antibody mimics, have been proved to be very promising candidates as highly selective adsorbents, due to their inherent advantages such as molecular specificity, reusability, physiochemical stability and applicability in harsh chemical media[24–26]. MIPs are typically synthesized by polymerization of functional monomers in the presence of a template molecule. Thereafter, the template is leached out, leaving behind cavities which are complementary in size, shape and functionality to the template. These "molecularly designed cavities" show an affinity for the template molecule over other structurally related compounds. Therefore, anti-interference ability of sensing element in complex matrices can be expected through integration of MIPs with a sensor[27–29]. On the other hand, high sensitivity and detection capacity are other common requirements in sensor industry[30–32] and it is easy to understand that a three-dimensional (3D) architecture with nanoscale features is superior to a flat, two-dimensional (2D) electrode surface in this case. Nanocarbon such as carbon nanotubes (CNTs)[33–35] and graphene[36] have been widely explored to modify planar electrode and commonly provide large surface area of the electrode/electrolyte interface. However, the resulted

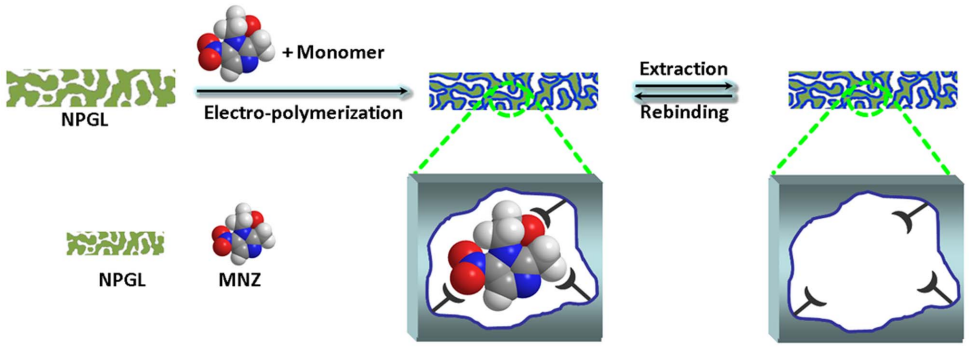

Figure 1 | **Schematic representation of MNZ-MIP/NPGL/GE fabrication.**

sensors may suffer from instability and poor reproducibility as a consequence of its modification process, where drop coating is often adopted and nanomaterials tend to distribute in a non-homogeneous manner. Electrodeposition of metal nanoparticles such as gold was also reported[37–42], but the overall performance and efficiency have to be negotiated by the way that nanoparticles stack with each other due to the poor controllability and stability during preparation.

Recently, nanoporous gold leaf (NPGL) has been demonstrated as a unique electrode for the development of new electrochemical sensors[43,44]. NPGL is a low-cost free-standing mesoporous thin film that can be mass-produced by dealloying commercially available Ag/Au alloy leaves[45]. Unlike gold particles, NPGL possesses a rigid 3D framework structure which avoids particle aggregation, thus improving the applicability and stability of the NPGL-based electrodes[46,47].

In this article, we report on the fabrication, characterization and application of a novel electrochemical sensor in which NPGL was decorated by an ultra-thin electro-synthesized MIP layer. The structures of thus produced electrochemical sensors were characterized and the experimental parameters influencing the performance of the sensors were investigated and optimized in detail. Moreover, the developed sensors were successfully employed for detecting MNZ in the pharmaceutical dosage form and real biological samples.

Results

In this study, MNZ is used as a detection model for the established nanohybrid electrochemical sensor, of which the fabrication procedure is illustrated in Figure 1. The electrodes were firstly characterized by SEM, which displays a type of sponge-like morphology with metal ligaments and quasi-periodic nanopore channels with characteristic width around 50 nm (Figure 2a). After electro-polymerization in the presence of monomer and template molecules, the NPGL was covered with a thin layer of polymer, leading to an obvious decrease in the width of the pore channels (Figure 2b).

Typical cyclic voltammograms obtained during the electro-polymerization are presented in Figure 3a. As suggested by the remarkable decrease of the current intensity under successive cyclic scans, a non-conducting film is formed, progressively covering the electrode surface and leading to the suppression of the voltammetric response. Figure 3b displays the cyclic voltammograms of different electrodes in the probe solution. Compared with bare gold electrode (GE), the current response of NPGL/GE increases evidently owing to its higher accessible surface area, which is very useful in elevating sensitivity. By

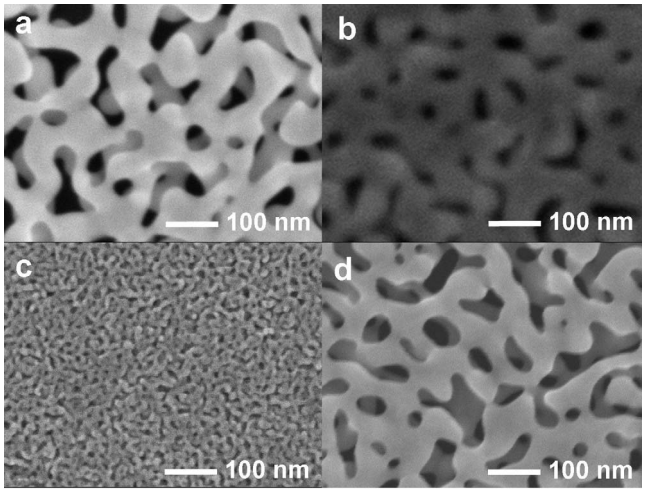

Figure 2 | **Characterization of different NPGL samples.** SEM images of (a) an NPGL sample after free dealloying in concentrated nitric acid for 60 min, (b) an MIP-covered NPGL sample obtain from free dealloying in concentrated nitric acid for 60 min, (c) an NPGL sample after potentiostatic dealloying in concentrated nitric acid for 1 min and (d) an NPGL sample after free dealloying in concentrated nitric acid for 24 h.

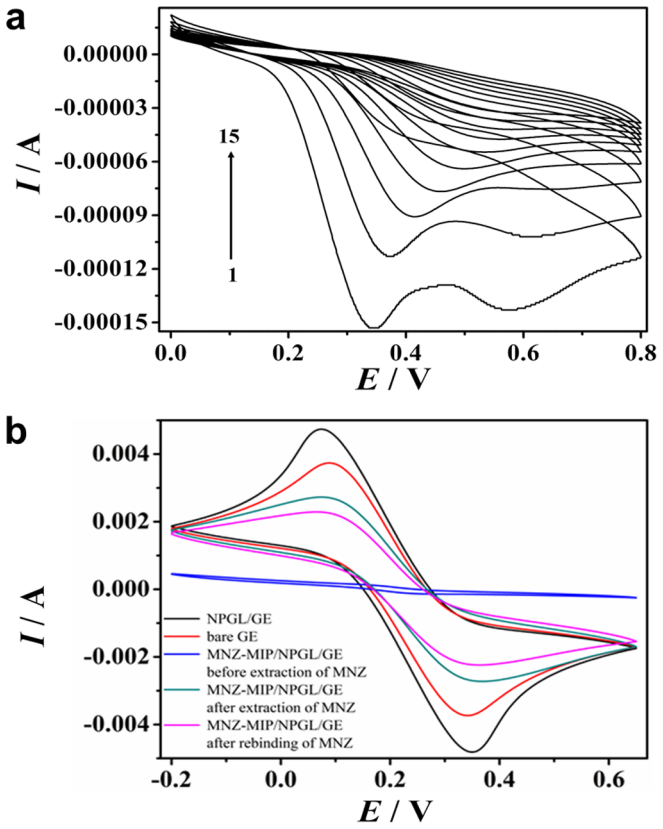

Figure 3 | (a) Cyclic voltammograms for the electrochemical polymerization of MNZ-MIP. (b) Cyclic voltammograms of different electrodes in the probe solution.

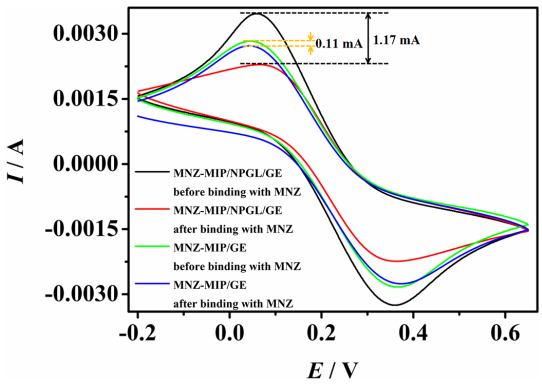

Figure 4 | Cyclic voltammograms of two different electrodes before and after binding with MNZ in the probe solution.

contrast, with existence of MNZ-embedding MIP film at the NPGL/GE surface, the pair of the redox peaks of the probe disappears. This can be explained by the fact that the polymeric film is not conductive and after the whole electrode surface was densely covered with the polymeric film, there was essentially no channel for the active probe to access the electrode surface. This also demonstrates a successful decoration of a thin layer of MNZ-MIP film onto the entire 3D surfaces of NPGL electrode.

After removing template from the electrode, the redox peak of the probe reappears, as template extraction left cavities in the rigid polymer matrix, which opened doors for the probe to transfer onto the electrode surface. Extraction of the template-MNZ was carried out by using diluted H_2SO_4 which could cause breakage of non-covalent interactions between the functional monomers and the template molecules. When the electrode was immersed in solution containing MNZ, rebinding of MNZ with MIP layer impeded the electron transfer of the $Fe(CN)_6^{3-/4-}$ ions on the electrode surface, resulting a decrease of the peak current. Apparently the rebinding process was mainly driven by the spatial structure complementation of imprinting cavities to MNZ molecules and the non-covalent interactions between MNZ and the residual functional groups in the polymer network[48]. Using the peak current shift (ΔI) for evaluating sensor's response to MNZ, we found that the sequence of response level was: MNZ-MIP/NPGL/GE > MNZ-MIP/GE ≫ NPGL/GE ≥ bare GE ≥ NIP/GE. Figure 4 exhibits cyclic voltammograms of the first two electrodes before and after binding with MNZ at the same concentration. It is obvious that the response of MNZ-MIP/NPGL/GE is much higher (by ~10.6 times) than that of MNZ-MIP/GE, implying the sensitivity enhancement provided by NPGL platform. The fact that bare GE and NPGL/GE hardly adsorbed any MNZ further proved that the efficient binding ability could be credited to the high recognition of MNZ-MIP film. Similarly, immersing NIP/GE in MNZ solution gave rise to imperceptible change in the current shift of $Fe(CN)_6^{3-/4-}$, which may be ascribed to the compact NIP film without imprinted cavities or other access available for probe ions to transfer to the electrode surface.

The optimal functional monomer was selected among the commonly used monomers during MIP preparation, including *o*-phenylenediamine, resorcinol, dopamine and *o*-aminophenol. These candidates were polymerized under their own practicable pH values. All polymerization occurred on the surface of bare GE with a molar ratio of 1 : 3 for template and monomer (T : M). After polymerization and extraction of template, the electrodes decorated with different MIP films were employed for detection of MNZ at the same concentration and their peak current shifts were calculated for evaluating the response level. Table 1 lists the reduction peak current shift obtained from different MIP/GE before and after exposure to MNZ. The optimum pH values for each monomer were selected in accordance with the highest current shift. As can be seen, the optimal pH values for *o*-phenylenediamine, resorcinol, dopamine and *o*-aminophenol are 6.0, 5.5, 7.0 and 1.1, respectively. Subsequently, the most appropriate ratio of MNZ to each monomer was explored by the same method under their optimum pH. Table 2 exhibits that the most ideal ratios (T : M) for the four MIP/GEs range from 1 : 2 to 1 : 4. Generally, in the preparation of non-covalent MIPs, an excess of functional monomer is usually introduced in order to maximize the formation of template-monomer assemblies[49]. However, excessive monomers can also result in a large number of polymer chains without template molecules incorporated, thereby blocking off the access to electrode and decreasing the efficiency of electron transfer. Moreover, sensors prepared with *o*-phenylenediamine (pH=6.0, T : M=1 : 2) and *o*-aminophenol (pH=1.1, T : M=1 : 4) as monomers show higher response to MNZ in comparison with those by employing other monomers. However, the pH of polymerization reaction for *o*-aminophenol is very low. Upon consideration of security and economic rationality, *o*-phenylenediamine was selected as function monomer for the following experiments. The illustration concerning the elution and rebinding of MNZ in the MIP matrix generated by *o*-phenylenediamine is displayed in Figure 5. As mentioned earlier, non-covalent interactions, including hydrogen bonds between amino group in polymer and nitro group in MNZ, electrostatic forces between amino groups in polymer and hydroxyl in MNZ and van der Waals force, are supposed to be the main driving forces for the modified sensor in recognizing MNZ.

Under the optimal analytical conditions, the determination of MNZ at different concentrations was performed by CV. Figure 6 illustrates the reduction peak current decreases linearly with increasing concentration of MNZ. The calibration curve shows dual linear relationships over MNZ concentration in the range of $5 \times 10^{-11} \sim 1 \times 10^{-9}$ mol L^{-1} and $1 \times 10^{-9} \sim 1.4 \times 10^{-6}$ mol L^{-1}, and the corresponding linear regression equations are ΔI (mA) = 0.3027 + 214.53 C (μM) (R^2 = 0.9910) and ΔI (mA) = 0.5071 + 0.2522 C (μM) (R^2 = 0.9988), respectively. Based on the signal-to-noise ratio of 3 : 1, the limit of detection (LOD) was estimated to be 1.8×10^{-11} mol L^{-1}. The ultralow detection limit may be attributed to the unique merits of NPGL. Its characteristic sponge-like open-cell foam morphology[43] makes it a high-surface-area material, allowing for much more active sites available for binding with MNZ. Secondly, immobilization of NPGL onto GE improves the electron transfer on

Table 1 | Optimization of pH value in reaction system with different monomers

	pH													
Monomer [a]	0.5	0.7	0.9	1.1	1.3	4.0	4.5	5.0	5.5	6.0	6.5	7.0	7.5	8.0
1	-[b]	-	-	-	-	-	-	0.0476	0.0767	0.1370	0.1050	0.0963	0.0311	-
2	-	-	-	-	-	0.0700	0.1097	0.1001	0.1301	0.0404	-	-	-	-
3	-	-	-	-	-	-	-	-	-	0.0273	0.1307	0.1748	0.3624	0.1699
4	0.0248	0.0097	0.1036	0.1394	0.0193	-	-	-	-	-	-	-	-	-

[a] 1: *o*-phenylenediamine, 2: resorcinol, 3: dopamine, 4: *o*-aminophenol;
[b] - refers that polymerization was unable to take place under this condition.

Table 2 | Optimization of molar ratio of template and monomer under optimum pH value

Condition	1:1	1:2	1:3	1:4	1:5	1:6
o-phenylenediamine pH=6.0	0.1642	0.3124	0.2006	0.1380	0.1630	0.1699
resorcinol pH=5.5	0.0730	0.1637	0.0923	0.0532	0.0237	0.0061
dopamine pH=7.0	0.0387	0.0783	0.1341	0.0527	0.0423	0.0165
o-aminophenol pH=1.1	0.0311	0.0582	0.1624	0.4210	0.1534	0.0929

sensor surface, consequently enhancing sensitivity. In comparison with other reported sensors for MNZ determination (Table 3), MNZ-MIP/NPGL has wider linear range and lower detection limit.

It is worth mentioning that the relationship among pore size, surface area of NPGL and sensitivity of the modified hybrid senor has also been investigated. Three kinds of NPGL with pore size around 15, 50 and 60 nm were tested and their morphology is exhibited in Figure 2. For the same film thickness, a coarsened structure usually shows lower surface area, which in turn points to a reduced sensitivity. Our results indeed follow this trend, and the LOD (S/N=3) of the three modified electrodes in sensing MNZ is 1.3×10^{-11}, 1.8×10^{-11} and 2.7×10^{-11} mol L^{-1}, respectively. However, even though NPGL with pore size about 15 nm led to slightly enhanced sensitivity, the resultant leaf was very brittle and thus less suitable to be used as a support.

To evaluate the reproducibility of the sensor, a series of MNZ solutions at three different concentrations (2×10^{-7}, 6×10^{-7} and 1×10^{-6} mol L^{-1}) were detected by using the same modified electrode. The relative standard deviation (RSD) of the measurements was less than 0.8% for four successive assays, reflecting the precision and reproducibility of the proposed sensor were quite good. To study the long-term stability of the sensor, the current response of MNZ-MIP/NPGL/GE towards MNZ was gauged every day for continuous 10 days, giving rise to an RSD of 0.66%. The sensor was stored at room temperature when not in use, and no apparent change in signals of MNZ detection was found after 15 days. It is suggested that the firm adhesion of NPGL onto GE, as well as the stable feature of both NPGL and MIP layer, is crucial in keeping the stability of the prepared sensor.

Selectivity of the modified sensor for MNZ was evaluated by investigating the sensor response in exposure to ronidazole, 4-nitroimidazole, 1,2-dimethylimidazole and dimetridazole, which are structurally similar to MNZ (Figure 7). Figure 8 shows that all the analogues caused much less response than MNZ did, suggesting the modified sensor exhibited excellent selectivity for the detection of MNZ and the cavities in imprinted polymer for recognition of the target molecules indeed formed.

Moreover, the main interferences existing in monitoring MNZ in real samples were surveyed. Starch, sucrose and dextrin, regarded as the major interfering substances in MNZ tablet, and glucose, Ca^{2+}, NH_4^+, Na^+, K^+, Cl^- and NO_3^-, as main interferents in biological sample (such as fish tissue) were detected together with MNZ, where concentrations of all the interferents were 10 times higher than that of MNZ. Compared with MNZ alone, the mixtures of MNZ and coexisting substances in tablet and fish tissue gave response of 104.3 and 103.6%, respectively.

To further explore the practical application of sensor, the determination of MNZ in tablet and fish tissue were carried out with the developed sensors using the standard addition method. Recovery, often used for evaluating the accuracy of developed assay method, was calculated via dividing the difference between measured quantity of MNZ in spiked sample and measured quantity of MNZ in non-spiked sample by the quantity of MNZ spiked. The recoveries were in the range of 98.2 to 105.9% for MNZ tablet assay (Table 4) and 99.2 to 105.9% for fish tissue analysis (Table 5). It is worth mentioning that high-performance liquid chromatography (HPLC) was also employed as a reference to statistically validate the established approach in detecting MNZ. As displayed in Table 6, there is an excellent agreement between the values obtained by our proposed methodology and the HPLC reference method, which evidently indicates that the system presented here is valid for real sample analysis.

Discussion

Here we have proposed a novel strategy where MIP/NPGL composite films were adopted for the fabrication of reusable electrochemical sensors that exhibited outstanding performance and practical usability. MNZ was successfully detected as a model compound. Firstly, NPGL played a key role in the improvement of the sensing properties, which was confirmed by the results of ultra-low detection limit. The 3D open and continuous nanoporous architecture provided large specific surface area, helping loading MIP and enhancing electronic transmission. Secondly, in situ electrochemical polymerization of MIP layer has been proved to be an attractive way of modifying electrodes due to several reasons: a) the preparation procedure is simple and quick, and film thickness is controllable by varying the amount of monomer deposited; b) formation of monomer network chains occurs directly on electrode surface, guaranteeing the good adherence of the MIP film onto the surface; c) the electro-synthesized MIP films are often shown as ultrathin layers[22,50], which ensure fast uptake/desorption process of analytes, thus shortening the detection time; d) since here polymerization proceeds in aqueous electrolyte solutions, measurement could also be taken in aqueous media, which is usually a bottleneck with conventional MIPs as water often damages the non-covalent interaction between polymer and template[48,51].

In addition, the admirable selectivity is believed to be ascribed to the synergistic effect of NPGL and MIP. On the one hand, the porous structure ensures the larger surface area of NPGL platform, signifi-

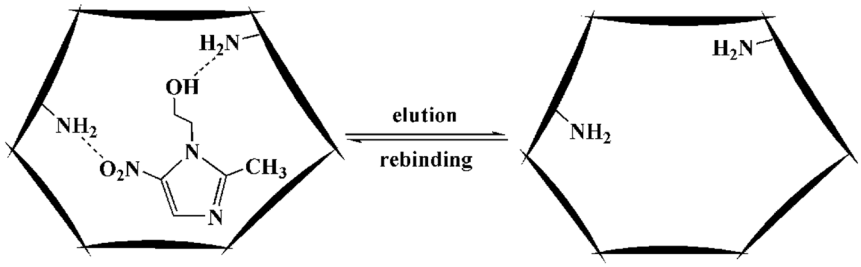

Figure 5 | Schematic diagram of elution and rebinding of MNZ in the MIP matrix generated by *o*-phenylenediamine.

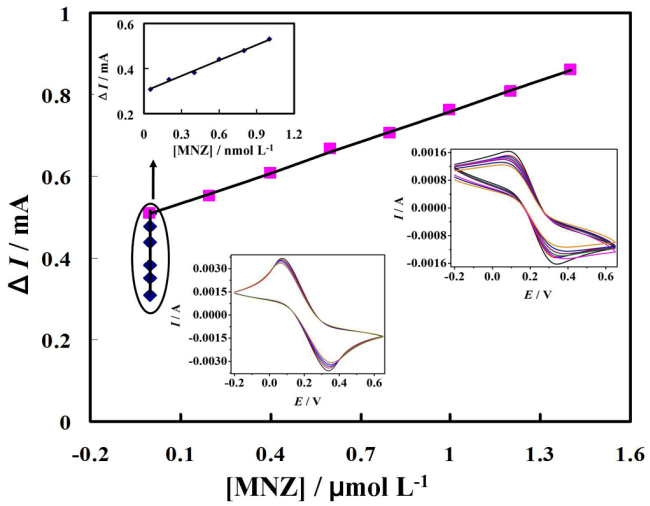

Figure 6 | The calibration curves for MNZ detection correlating reduction peak current shift with MNZ concentration, by the use of MNZ-MIP/NPGL/GE. The calibration curve in top-left inset is obtained with MNZ concentration in the range of 5×10^{-11} to 1×10^{-9} mol L^{-1} and the cyclic voltammograms in accordance is in bottom-left inset, while the bottom-right inset shows cyclic voltammograms with MNZ concentration in the range of 1×10^{-9} to 1.4×10^{-6} mol L^{-1}.

cantly elevating the amount of imprinted sites, consequently boosting the binding capacity (Figure 4). On the other hand, MIP recognizes MNZ molecules by means of shape and size matching, as well as interaction between functional groups ($-NH_2$, $-OH$) in the polymeric network and MNZ, where hydrogen bonding might be the main force in driving molecular adsorption (Figure 5). Since other analogues and interferents do not match with the template-imprinted cavities, the hybrid sensor is endued with satisfying anti-interference capability in detecting analytes of interest in complicated media.

In the perspective of adsorption equilibrium characterization, two kinds of affinity binding sites may exist, which could explain the appearance of double-linearity when the as prepared sensor was exposed to analyte (Figure 6). At low concentration, substrates prefer to occupy the binding sites of high affinity on sensor surface, while at high concentration, after the high affinity sites are gradually taken up, further combination takes place between the substrates and the low affinity binding sites. Apparently the latter process is harder for molecules to overcome transfer resistance and get in touch with the internal cavities than the former. Generally speaking, different affinity binding sites provided by the same adsorbent bring about different equilibrium dissociation constants, thereby leading to disparate equilibrium adsorption capacity[52]. As a result, a sensor may demonstrate different responses over different analyte concentration ranges. In-depth studies are apparently required to clarify the underlying mechanisms in molecular level.

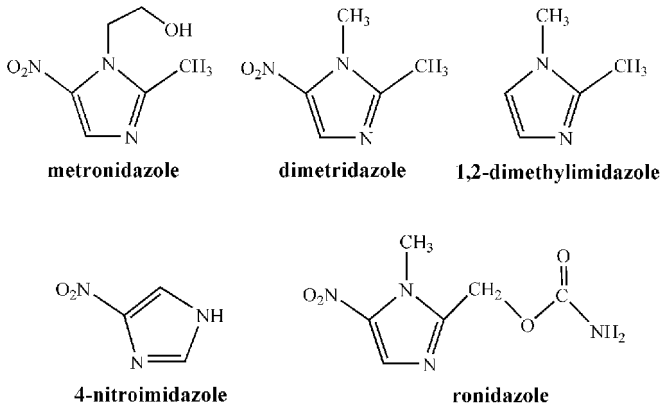

Figure 7 | Chemical structures of MNZ and its structural analogues.

In summary, by utilizing a facile two-step coating procedure involving NPGL modification and MIP electro-polymerization, we have developed a highly sensitive and selective electrochemical sensing protocol for the detection of MNZ. This is to our knowledge the first report on coupling of molecular imprinting technology and nanoporous gold leaf technique for establishing advanced sensing devices. Further experiments are in progress in order to extend the applications of these hybrid nanoarchitectures for ultra-sensitive detection of other analytes.

Methods

Chemicals and instruments. Metronidazole (MNZ), ronidazole, 4-nitroimidazole, 1,2-dimethylimidazole, dimetridazole, *o*-phenylenediamine, resorcinol and o-aminophenol were purchased from Shanghai Aladdin Co. (Shanghai, China). Au/Ag alloy leaves (50 : 50 wt%; 100 nm in thickness) were obtained from Suzhou ColdStones Tech. Co. Ltd. (Suzhou, China). Dopamine was obtained from Shanghai Jianglai Reagent Co. (Shanghai, China). MNZ tablet (each containing 200 mg MNZ) was purchased at local drugstore. Crucian fish was obtained at local market. Reagents and materials, such as starch, sucrose, dextrin glucose, $Fe(CN)_6^{3-/4-}$, $CaCl_2$, NH_4Cl, NaCl, KNO_3, H_2SO_4, HNO_3, methanol and phosphate buffer solution (PBS, KH_2PO_4 and K_2HPO_4) were of analytical grade. All solutions were prepared using double distilled water.

Electrochemical measurements were performed on a CHI 760E Electrochemical Workstation (CHI Instruments Co., Shanghai, China) connected to a PC at room

Table 3 | Comparison of the major characteristics of literature methods used for MNZ detection

Method	Dynamic range (μmol L^{-1})	LOD (μmol L^{-1})	RSD (%)	References
Fe_3O_4/SiO_2-MIP/magnetic GCE	0.05–1.0	0.016	4.8	4
Graphene-ionic/liquid/GCE	0.1–25.0	0.047	2.1	15
Single-walled carbon nanotube/GCE	0.1–200	0.063	-	16
Carbon fiber microdisk electrode	5.0–16.0	0.5	3.7	12
Gold electrode	0.001–2	0.0001	1.84	14
MIP/carbon paste electrode	0.00033–0.45	0.00021	<4.0	13
Cysteic acid/PDDA-GN[a]/GCE[b]	0.01–1	0.0023	3.3	5
Co/GCE[b]	0.4–100	0.2	-	18
Stripping voltammetry of MNZ	0.01–1.0	0.0025	-	17
MIP modified pencil graphite electrode	5.77×10^{-5}–760	5.84×10^{-6}	1.8	20
Ni/Fe-layered double hydroxides/GCE	5–1610	58	<4.0	19
Magnetic-MIP/graphene/GCE	3.2×10^{-2}–3.4	1.2×10^{-3}	7.8	21
This work	5×10^{-5}–1.4	1.8×10^{-5}	0.8	-

[a]GCE refers to glassy carbon electrode.
[b]PDDA-GN refers to poly (diallydimethylammonium chloride)-functionalized graphene.

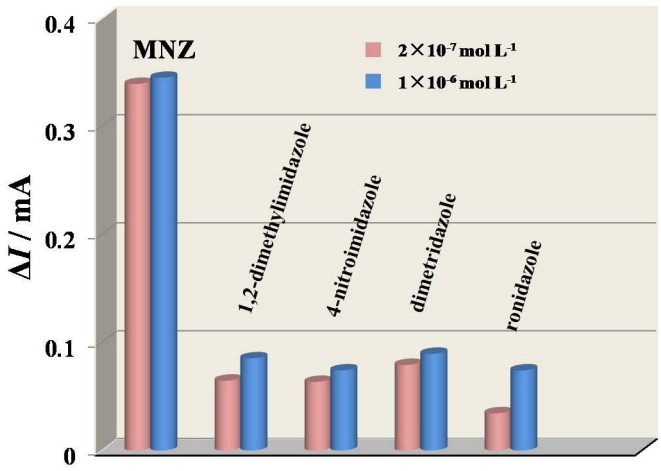

Figure 8 | Determination of MNZ and some of its structural analogues at two different concentrations by using MNZ-MIP/NPGL/GE.

as-received alloy leaves were cut into 6 × 6 mm pieces and transferred onto the surface of concentrated nitric acid (65 vol%). The etching was stopped after 60 min, and then the sample was rinsed with distilled water thoroughly. In comparison, two other leaves with different pore size were also produced by potentiostatic dealloying for 1 min under 0.6 V and by free corrosion for 24 h in nitric acid (65 vol%).

Fabrication of electrochemical sensor. GE was first polished repeatedly to a mirror finish with 0.3 and 0.05 μm Al_2O_3 and thoroughly cleaned with distilled water before use. Then NPGL was carefully affixed to GE surface and the NPGL-modified GE (NPGL/GE) was dried under infrared lamp for 20 min. Electro-polymerization of MIPs in the presence of MNZ on the electrode surface was realized by cyclic voltammetry (CV), which was performed between 0 and +0.8 V (vs. SCE) for 15 cycles at a scan rate of 50 mV s^{-1} in a solution containing functional monomers and MNZ. The NPGL/GE bearing the polymer film was immersed in 0.3 mol L^{-1} H_2SO_4 to extract embedded MNZ by scanning between −1.0 ~ +1.0 V for several cycles until no obvious redox peak could be observed in the probe solution (containing 0.01 mol L^{-1} KNO_3 and 0.05 mol L^{-1} $Fe(CN)_6^{3-/4-}$). The schematic representation for the preparation of MNZ-MIP/NPGL/GE is illustrated in Scheme 1. As a control, non-imprinted polymer (NIP)-modified electrode, named as NIP/GE, was prepared by the same procedure but in the absence of the template MNZ during electro-polymerization.

Electrochemical measurement. Electrochemical behavior of different electrodes was investigated using cyclic voltammetric technique in 25 mL probe solution. The changes of peak current intensity of $Fe(CN)_6^{3-/4-}$ were tracked to evaluate the

Table 4 | Determination of MNZ in tablet by using MNZ-MIP/NPGL/GE (n=3)

Labeled amount of MNZ (mg)	Measurement value of sample (mg)	Spiked (mg)	Measurement value of total (mg)	Recovery (%)	RSD (%)
250	245.5 ± 8.1	-	-	98.2	3.3
250	245.5 ± 8.1	200.1	445.9 ± 9.8	100.1	2.2
250	245.5 ± 8.1	250.4	510.7 ± 9.2	105.9	1.8
250	245.5 ± 8.1	300.2	555.0 ± 17.2	103.1	3.1

Mean value ± S.D.

Table 5 | Determination of MNZ in fish tissue by using MNZ-MIP/NPGL/GE (n=3)

Measurement value of sample (mg)	Spiked (mg)	Measurement value of total (mg)	Recovery (%)	RSD (%)
0.0762 ± 0.0016	-	-	-	2.1
0.0762 ± 0.0016	0.0609	0.1407 ± 0.0038	105.9	2.7
0.0762 ± 0.0016	0.0762	0.1518 ± 0.0049	99.2	3.2
0.0762 ± 0.0016	0.0914	0.1691 ± 0.0029	101.6	1.7

Mean value ± S.D.

temperature. A conventional three-electrode system was employed, consisting of a bare or a modified planar gold electrode (GE, 4 mm in diameter) as the working electrode, a saturated calomel electrode (SCE) as the reference electrode and a platinum wire (0.5 mm in diameter, 34 mm in length) as the counter electrode. All potentials given in this paper were referred to SCE. The surface morphology of NPGL was characterized with a Nova Nano SEM 450 field emission scanning electron microscope operating at 10 kV.

The high–performance liquid chromatography (HPLC) was performed using an Essentia LC–15C system equipped with two LC–15C Solvent Delivery Units, an LC Solution 15C workstation and an SPD–15C UV–Vis Detector (Shimadzu, Japan). LC condition was as follows: chromatographic separation was performed on a Shimadzu WondaSil C18 column (150 mm × 4.6 mm i.d., 5 μm). The mobile phase was methanol–water (2 : 8, v/v) with a flow rate of 1.0 mL/min, and the detection wavelength was set at 315 nm. A KQ3200E ultrasonic cleaner (Kunshan Instrument Co., Jiangsu, China) was set at 40 kHz. All measurements were performed in triplicate.

Preparation of NPGL. Nanoporous gold leaf (NPGL) was prepared by selectively dealloying Ag from Ag/Au alloy leaves, similar to that reported in ref. 45. Briefly, the

influence of different modification on sensor behavior and to analyze the binding action of the modified sensor to MNZ or other substances.

The determination procedure is as follows. A sensor was incubated in a sample solution containing analyte for 5 min at room temperature, after which the electrode was washed with water and applied for voltammetric measurement. The scan was performed from −0.2 to +0.65 V at a rate of 100 mV s^{-1}. The current shift (ΔI) was used to evaluate the binding capacity of sensor and it was calculated from the reduction peak currents obtained before and after combination with MNZ. In general, a washing step was followed after detection of one kind of analyte to extract adsorbed compounds, where the modified electrode was immersed in H_2SO_4 upon scanning between −1.0 ~ +1.0 V for several cycles until no obvious redox peak could be observed. Then the modified electrode was incubated in the next analyte for the following survey.

Detection of MNZ in tablet form and in biological sample. MNZ tablets were grounded to fine powder and a portion of the powder was accurately weighed and dissolved with methanol. After 5 min of ultra-sonication, the solution was filtered and the filtrate was quantitatively diluted to a certain concentration with methanol for

Table 6 | Comparison for the determination of MNZ in real samples by using HPLC and the modified sensor

	Sample of tablet (Theory value of MNZ is 0.16 μg mL^{-1})		Sample of fish tissue (Theory value of MNZ is 0.08 μg mL^{-1})	
Method	Measurement value (μg mL^{-1})	Recovery (%)	Measurement value (μg mL^{-1})	Recovery (%)
this work	0.1725	107.8	0.0849	106.1
HPLC	0.1668	104.2	0.0821	102.6

subsequent determination of MNZ. For the spiked recovery experiment, a certain amount of MNZ was added into the tablet powder and the same treatment was followed as described above.

As for monitoring MNZ in fish meat, a healthy crucian carp fasted first for 24 h, and was given a certain quantity of MNZ mixed in feed. After feeding 48 h, 2.0 g fish meat with fish-skin and bones removed was taken and homogenized with 7 ml methanol. Afterwards, the homogenate was mixed with methanol in a volumetric ratio of 1 : 1 to get rid of protein, followed by centrifugation. The supernatants were used for assaying MNZ. For the spiked recovery experiment, a certain amount of MNZ was added in the samples during homogenization.

1. Edwards, D. The action of metronidazole on DNA. *J. Antimicrob. Chemoth.* **3**, 43–48 (1977).
2. Tally, F. P. & Sullivan, C. E. Metronidazole: in vitro activity, pharmacology and efficacy in anaerobic bacterial infections. *J. Hum. Pharmacol. Drug Ther.* **1**, 28–38 (1981).
3. Bucklin, M. H., Groth, C. M. & Henriksen, B. *Encyclopedia of Toxicology,* Edn. 3rd. 330–331 (Academic Press, Salt Lake City, USA, 2014).
4. Chen, D. *et al.* A core-shell molecularly imprinted polymer grafted onto a magnetic glassy carbon electrode as a selective sensor for the determination of metronidazole. *Sensor. Actuator. B: Chem.* **183**, 594–600 (2013).
5. Liu, W. *et al.* A novel composite film derived from cysteic acid and PDDA-functionalized graphene: enhanced sensing material for electrochemical determination of metronidazole. *Talanta* **104**, 204–211 (2013).
6. U.S. Food and Drug Administration, *Prohibited and restricted drugs in food animals from Food animal residue avoidance databank. Regulatory information.* (2014) Available at: http://www.farad.org/eldu/prohibit.asp (Accessed: 6th June 2014)
7. International Agency for Research on Cancer of World Health Organization, *Agents classified by the IARC monographs. List of classifications.* (2014) Available at: http://monographs.iarc.fr/ENG/Classification/index.php (Accessed: 2nd June 2014)
8. Mishal, A. & Sober, D. Stability indicating reversed-phase liquid chromatographic determination of metronidazole benzoate and diloxanide furoate as bulk drug and in suspension dosage form. *J. Pharmaceut. Biomed.* **39**, 819–823 (2005).
9. Erk, N. & Altun, M. L. Spectrophotometric resolution of metronidazole and miconazole nitrate in ovules using ratio spectra derivative spectrophotometry and RP-LC. *J. Pharmaceut. Biomed.* **25**, 115–122 (2001).
10. Fabayo, A. & Grudziński, S. Quality control of drugs. III. Quantitative determination of metronidazole in tablets by UV-absorption spectrophotometry. *Acta Pol. Pharm.* **42**, 49–54 (1984).
11. Tan, S., Jiang, J., Yan, B., Shen, G. & Yu, R. Preparation of a novel fluorescence probe based on covalent immobilization by emulsion polymerization and its application to the determination of metronidazole. *Anal. Chim. Acta* **560**, 191–196 (2006).
12. Bartlett, P. N., Ghoneim, E., El-Hefnawy, G. & El-Hallag, I. Voltammetry and determination of metronidazole at a carbon fiber microdisk electrode. *Talanta* **66**, 869–874 (2005).
13. Gholivand, M. B. & Torkashvand, M. A novel high selective and sensitive metronidazole voltammetric sensor based on a molecularly imprinted polymer-carbon paste electrode. *Talanta* **84**, 905–912 (2011).
14. Mollamahale, Y. B., Ghorbani, M., Ghalkhani, M., Vossoughi, M. & Dolati, A. Highly sensitive 3D gold nanotube ensembles: Application to electrochemical determination of metronidazole. *Electrochim. Acta* **106**, 288–292 (2013).
15. Peng, J., Hou, C. & Hu, X. Determination of metronidazole in pharmaceutical dosage forms based on reduction at graphene and ionic liquid composite film modified electrode. *Sensor. Actuator. B: Chem.* **169**, 81–87 (2012).
16. Salimi, A., Izadi, M., Hallaj, R. & Rashidi, M. Simultaneous determination of ranitidine and metronidazole at glassy carbon electrode modified with single wall carbon nanotubes. *Electroanal.* **19**, 1668–1676 (2007).
17. Wang, Z., Zhou, H. & Zhou, S. Study on the determination of metronidazole in human serum by adsorptive stripping voltammetry. *Talanta* **40**, 1073–1075 (1993).
18. Zhi, Y., Hu, J., Wu, Z. & Li, Q. Study on the voltammetric behavior of metronidazole and its determination at a Co/GC modified electrode. *Anal. Lett.* **31**, 429–437 (1998).
19. Nejati, K. & Asadpour-Zeynali, K. Electrochemical synthesis of nickel-iron layered double hydroxide: application as a novel modified electrode in electrocatalytic reduction of metronidazole. *Mat. Sci. Eng. C-Mater.* **35**, 179–184 (2014).
20. Roy, E., Maity, S. K., Patra, S., Madhuri, R. & Sharma, P. K. A metronidazole-probe sensor based on imprinted biocompatible nanofilm for rapid and sensitive detection of anaerobic protozoan. *RSC Adv.* **4**, 32881–32893 (2014).
21. Yang, G., Zhao, F. & Zeng, B. Magnetic entrapment for fast and sensitive determination of metronidazole with a novel magnet-controlled glassy carbon electrode. *Electrochim. Acta* **135**, 154–160 (2014).
22. Liu, Y. *et al.* Fabrication of highly sensitive and selective electrochemical sensor by using optimized molecularly imprinted polymers on multi-walled carbon nanotubes for metronidazole measurement. *Sensor. Actuator. B: Chem.* **206**, 647–652 (2015).
23. Kong, L., Pan, M., Fang, G., Qian, K. & Wang, S. An electrochemical sensor for rapid determination of ractopamine based on a molecularly imprinted electrosynthesized o-aminothiophenol film. *Anal. Bioanal. Chem.* **404**, 1653–1660 (2012).
24. Haginaka, J. Molecularly imprinted polymers as affinity-based separation media for sample preparation. *J. Sep. Sci.* **32**, 1548–1565 (2009).
25. Mayes, A. G. & Mosbach, K. Molecularly imprinted polymers: useful materials for analytical chemistry? *Trac-Trend. Anal.Chem.* **16**, 321–332 (1997).
26. Wu, W. *et al.* Specific glucose-to-SPR signal transduction at physiological pH by molecularly imprinted responsive hybrid microgels. *Biomaterials* **33**, 7115–7125 (2012).
27. Afkhami, A., Ghaedi, H., Madrakian, T., Ahmadi, M. & Mahmood-Kashani, H. Fabrication of a new electrochemical sensor based on a new nano-molecularly imprinted polymer for highly selective and sensitive determination of tramadol in human urine samples. *Biosens. Bioelectron.* **44**, 34–40 (2013).
28. Piletsky, S. A. & Turner, A. P. Electrochemical sensors based on molecularly imprinted polymers. *Electroanal.* **14**, 317–323 (2002).
29. Xie, C., Gao, S., Guo, Q. & Xu, K. Electrochemical sensor for 2,4-dichlorophenoxy acetic acid using molecularly imprinted polypyrrole membrane as recognition element. *Microchim. Acta* **169**, 145–152 (2010).
30. Korotcenkov, G. & Cho, B. K. Engineering approaches for the improvement of conductometric gas sensor parameters: Part 1. Improvement of sensor sensitivity and selectivity (short survey). *Sensor. Actuator. B: Chem.* **188**, 709–728 (2013).
31. Li, Y., Lucklum, R., Brose, A. & Fleischer, M. A 2-step coating technique for CMUT based chemical sensors. *Sensor. Actuator. B: Chem.* **161**, 171–177 (2012).
32. Prakash, S., Chakrabarty, T., Singh, A. K. & Shahi, V. K. Polymer thin films embedded with metal nanoparticles for electrochemical biosensors applications. *Biosens. Bioelectron.* **41**, 43–53 (2013).
33. Rezaei, B. & Rahmanian, O. Nanolayer treatment to realize suitable configuration for electrochemical allopurinol sensor based on molecular imprinting recognition sites on multiwall carbon nanotube surface. *Sensor. Actuator. B: Chem.* **160**, 99–104 (2011).
34. Rezaei, B., Rahmanian, O. & Ensafi, A. A. An electrochemical sensor based on multiwall carbon nanotubes and molecular imprinting strategy for warfarin recognition and determination. *Sensor. Actuator. B: Chem.* **196**, 539–545 (2014).
35. Yang, G., Zhao, F. & Zeng, B. Electrochemical determination of cefotaxime based on a three-dimensional molecularly imprinted film sensor. *Biosens. Bioelectron.* **53**, 447–452 (2014).
36. Ge, S. *et al.* Electrochemical biosensor based on graphene oxide-Au nanoclusters composites for l-cysteine analysis. *Biosens. Bioelectron.* **31**, 49–54 (2012).
37. Celik, E., Keskin, I., Kayatekin, I., Azem, F. A. & Özkan, E. Al_2O_3-TiO_2 thin films on glass substrate by sol-gel technique. *Mater. Charact.* **58**, 349–357 (2007).
38. Syres, K., Thomas, A., Bondino, F., Malvestuto, M. & Grätzel, M. Dopamine adsorption on anatase TiO_2 (101): A photoemission and NEXAFS spectroscopy study. *Langmuir*, **26**, 14548–14555 (2010).
39. Zhu, A., Tian, Y., Liu, H. & Luo, Y. Nanoporous gold film encapsulating cytochrome c for the fabrication of a H_2O_2 biosensor. *Biomaterials* **30**, 3183–3188 (2009).
40. Zhang, X. *et al.* A novel electrochemical sensor based on electropolymerized molecularly imprinted polymer and gold nanomaterials amplification for estradiol detection. *Sensor. Actuator. B: Chem.* **200**, 69–75 (2014).
41. Xu, S. & Han, X. A novel method to construct a third-generation biosensor: self-assembling gold nanoparticles on thiol-functionalized poly(styrene-co-acrylic acid) nanospheres. *Biosens. Bioelectron.* **19**, 1117–1120 (2004).
42. Xie, C., Li, H., Li, S., Wu, J. & Zhang, Z. Surface molecular self-assemblyfor organophosphate pesticide imprinting in electropolymerized poly(p-aminothiophenol) membranes on a gold nanoparticle modified glassy carbonelectrode. *Anal. Chem.* **82**, 241–249 (2012).
43. Scanlon, M. D. *et al.* Characterization of nanoporous gold electrodes for bioelectrochemical applications. *Langmuir* **28**, 2251–2261 (2012).
44. Ding, Y. & Chen, M. Nanoporous metals for catalytic and optical applications. *MRS Bull.* **34**, 569–576 (2009).
45. Ding, Y., Kim, Y. J. & Erlebacher, J. Nanoporous gold leaf: "Ancient technology"/ advanced material. *Adv. Mater.* **16**, 1897–1900 (2004).
46. Ciesielski, P. N. *et al.* Functionalized nanoporous gold leaf electrode films for the immobilization of photosystem I. *ACS Nano* **2**, 2465–2472 (2008).
47. Wei, Q. *et al.* Nanoporous gold film based immunosensor for label-free detection of cancer biomarker. *Biosens. Bioelectron.* **26**, 3714–3718 (2011).
48. Haupt, K. Molecularly imprinted polymers in analytical chemistry. *Analyst* **126**, 747–756 (2001).
49. Li, Y., Fu, Q., Zhang, Q. & He, L. Preparation and evaluation of uniform-size (-)-ephedrine-imprinted polymeric microspheres by multi-step swelling and suspension polymerization. *Anal. Sci.* **22**, 1355–1360 (2006).
50. Apodaca, D. C., Pernites, R. B., Ponnapati, R. R., Del Mundo, F. R. & Advincula, R. C. Electropolymerized molecularly imprinted polymer films of a bis-terthiophene dendron: folic acid quartz crystal microbalance sensing. *ACS Appl. Mater. Inter.* **3**, 191–203 (2010).
51. Lin, L. *et al.* Preparation of molecularly imprinted polymer for sinomenine and study on its molecular recognition mechanism. *Polymer* **47**, 3792–3798 (2006).

52. Fletcher, J. E., Spector, A. A. & Ashbrook, J. D. Analysis of macromolecule-ligand binding by determination of stepwise equilibrium constants. *Biochemistry* **9**, 4580–4587 (1970).

Acknowledgments

The project was financially sponsored by the Doctor Foundation of Xinjiang Bingtuan (No. 2012BB020), the National 973 (No. 2012CB932800) Program Project of China, National Natural Science Foundation of China (No. 81260487, 51171092), the Scientific Research Foundation for the Returned Overseas Chinese Scholars from Ministry of Human Resources and Social Security of China (No. RSLX201301). Y.D. also acknowledges the Otto Mønsteds Fond for a visiting professorship at the Technical University of Denmark (DTU).

Author contributions

Y.C.L. and Y.D. designed this research; Y.L. and J.L. fabricated the sensor. Y.L. and J.L. performed the sensing experiments and processing of the data. H.T., C.C. and D.S.Z. jointly analyzed the data. All authors contributed to the discussion of the results. Y.C.L., Y.L. and Y.D. wrote the paper.

Additional information

Competing financial interests: The authors declare no competing financial interests.

How to cite this article: Li, Y. *et al.* Molecularly imprinted polymer decorated nanoporous gold for highly selective and sensitive electrochemical sensors. *Sci. Rep.* **5**, 7699; DOI:10.1038/srep07699 (2015).